Estimates of the Suprathermal O^+ outflow characteristic energy and relative location in the auroral oval

L. Andersson, W. K. Peterson and K. M. McBryde

Laboratory for Atmospheric and Space Physics, University of Colorado, Boulder, Colorado, USA

Abstract

We have surveyed one year of northern hemisphere data from the FAST satellite and obtained the first global estimates of the characteristic energy of the energetic oxygen ion outflows and their relative distribution within the auroral oval. Recent results have shown that, above ~3,000 km, the FAST/TEAMS instrument covers the energy range that includes almost all of the escaping O^+. The highest mean characteristic O^+ energy is found at the poleward edge of the night-side auroral oval. Our results suggest that the energization and/or transport are operating differently in the noon, dusk, midnight and dawn sectors of the auroral oval. The results presented here also provide required ground truth and boundary conditions for global modeling.

Introduction

We know surprisingly little about the average energy of ionospheric ions participating in the large scale magnetospheric processes. This information is needed to improve models which can be used to systematically explore possible mechanisms which relate ionospheric outflow and long time scale magnetospheric processes such as storms and substorms.

There have been numerous studies about the ion outflow rates from the ionosphere [see recent reviews by Yau and André, 1997; and Hultqvist *et al.,* 1999]. Cully *et al.,*

[2003]; and Lennartsson *et al.* [2004] have shown that the total escaping flux of O^+ observed on Akebono, DE –1 and Polar is constant with altitude.

The characteristic energy of the outflowing energetic ions at auroral latitudes has not been systematically studied. There have been reports on the evolution of ion conic pitch angles and energies as a function of altitude, indicating that ion heating takes place over a large altitude range [Peterson *et al.*, 1992; and Miyake *et al.*, 1996]. Peterson *et al.* [1995, Figure 14] reported that the characteristic energy of H^+, He^+, and O^+ conics increased only slightly (~100 eV) in the altitude range from 8000 to 24000 km using DE–1 data. Miyake *et al.* [1993, Figures 9 and 10] reported non-mass identified conic temperatures for the altitude range 2000 to 10000 km from Akebono. Lennartsson *et al.* [2004] discusses the differences in observed H^+ and O^+ characteristic energies observed between the perigee (~6000 km) and apogee (~60,000 km) for the Polar mission. These are the only reports we have been able to find of large-scale surveys of ion energy as a function of altitude.

Here we report on suprathermal ion outflow (ions > 3 eV), polar wind ions which have been energized above the auroral ionosphere. Specifically, we report the characteristic O^+ energies as function of altitude and relative position in the auroral zone.

Data

This study is based on data from the Time-of-flight Energy, Angle, Mass Spectrograph (TEAMS) instrument [Klumpar *et al.,* 2001] from the FAST mission [Carlson *et al.,* 1998]. We have examined the FAST data obtained at all local times in the altitude range from 1500 to 4200 km in 1997. The TEAMS instrument is fully three-dimensional and covers the energy range of ~3 eV-10 keV/q. One full ion distribution can be obtained after a half-spin, but in this study the highest time resolution used is one full spin, i.e. 5 seconds. The Electro Static Analyzers for Electrons (EESA) and Ions (IESA) [Carlson *et al.,* 2001] have been used to identify the auroral oval boundaries, as described by Andersson *et al*. [2004].

An example of data obtained by the FAST satellite is presented in Figure 1. From top to bottom, panels (a) and (b) present the anti-earthward (upward) and the earthward (downward) O^+ energy flux spectrogram, and the calculated characteristic energy E_{O+} (red and white curves) as described below. Panel (c) shows the calculated field upward

(red) and downward (black) O^+ number fluxes, which have been normalized to 300 km. The field aligned ion flux is derived from all pitch angles assuming that the mirroring population will give no net contribution as described by Andersson *et al.* [2004]. Panel (d) presents the calculated O^+ densities. The red vertical lines indicate the polar cap location identified from the electron measurement (EESA), as described in Andersson *et al.* [2004].

The characteristic anti-earthward center of energy ($E_{O+} = \Psi/J$) that is shown as a red line in Figure 1a is derived from the anti-earthward field-aligned (90-270° in Figure 1a) energy flux (Ψ) and the number flux (J). The absence of the red line corresponds to regions where the E_{O+} could not be determined by the algorithm described in the rest of this paragraph. The calculation of anti-earthward E_{O+} is only meaningful for distributions that have clear anti-earthward flow. We have restricted our analysis to distributions that satisfy the following criteria: 1) the density range was within 1-500 cm^{-3}; 2) there was a net anti-earthward energy flux; 3) the spacecraft potential was greater than -1 V; 4) the instrument was operating properly. These constraints are chosen to eliminate distributions affected by low altitude ram effect, spacecraft charging, and distributions of low statistical significance. The escaping O^+ Flux observed by the FAST satellite above 3000 km [Andersson *et al.,* 2004] equals that reported by Cully *et al.* [2003] and Lennartsson *et al.* [2004]. These reports justify our assumption that O^+ ions with energies less than 3 eV at altitudes above 3000 km do not contribute significantly to the escaping O^+ population. At lower altitudes the calculated E_{O+} is overestimated. The calculation of E_{O+} is also optimized to remove the effects of low signal levels and mirroring particles (examples of mirroring particles can be seen at the start and end of Figure 1a and 1b). A correction for the spacecraft potential is also made. To minimize the effects of low signal levels and mirroring particles, the energy range used to calculate E_{O+} is dynamically determined. The lower energy is always 3 eV and the upper energy is set to 500 eV or lower. The energy range is constrained because with no detectable fluxes above ~500 eV the instrumental noise will mimic an anomalous hot tail population and the calculated E_{O+} will be overestimated. Mirroring energetic O^+ from the plasma sheet will also increase the calculated $E_{O+.}$ To identify time periods when there is a mirror population of energetic O^+ present, the earthward E_{O+} is calculated first. When the earthward E_{O+}

(shown as a white line in Figure 1b) is low, the upper energy range selected for the anti-earthward E_{O+} calculation is set to 500 eV. A high value of the earthward E_{O+} indicates the presence of mirroring O^+, and for these cases the upper energy limit for calculating anti-earthward E_{O+} is lowered by an empirical expression. We have empirically determined that our algorithm produces reliable results for low to moderate E_{O+} (<100 eV) and it systematically underestimates E_{O+} for distributions with energetic ion conics. Note that ion beams that are typically observed in the cavity of 'inverted-Vs' have been systematically excluded from the database due to the selected density thresholds.

The O^+ mean characteristic energy

We have used the procedure outlined above to process data acquired by the FAST spacecraft in 1997 from the northern hemisphere. The resulting data are presented as a function of invariant latitude and magnetic local time in Figure 2 as described by Andersson *et al.,* [2004]. The data are presented for three different altitude ranges: 1500-2500, 2500-3200 and 3200-4200 km (columns). For each altitude range the following information are presented (from the top row to the bottom row): the mean E_{O+}, the mean net outflow derived from distributions in which it was possible to calculate E_{O+}, and the mean net O^+ outflow using all distributions (also including measurements outside the auroral oval). The large dials show the calculated result and the small dials show the number of events (distributions) in each of the pixels in the large dials. The data in Figure 2i are the most directly comparable to those presented by Andersson *et al.* [2004]. The minor differences presented here are consistent with the different altitude ranges and the other selection criteria used here. The total outflow of Figure 2g-i is ~2×10^{24} #/s, which is similar to other studies [Peterson *et al.*, 2001; Cully *et al.*, 2003; and Lennartsson *et al.,* 2004].

Figure 3 presents the ion outflow with respect to MLT and location of oval. The data in Figure 3a-c are the fraction of data in Figure 2a-c that are within the auroral oval. The data in Figure 3d-f are integrals over local time regions presented as line plots for four different MLT-regions: midnight (22-02 MLT), pre- and post-midnight (20-22 and 02-04 MLT), dawn/dusk (04-08 and 14-22 MLT), and noon (08-14 MLT). Figure 3g-i shows

the outflow flux with line plots of the four regions; the sampling statistics can be seen in the small dials of Figure 3a-c.

We were able to estimate the E_{O+} for only a small fraction of data intervals sampled. There were ~1.7 x 10^6 five-second data intervals sampled in 1997. 13% of these data intervals occurred in the auroral oval at the time the TEAMS instrument returned valid O^+ data. We were able to estimate the E_{O+} in ~20% (44000) of the total northern hemisphere auroral intervals with mass analysis and these are presented in Figure 2a-c and Figure 3a-c.

The average E_{O+} shown in Figure 3 is low. We found that 8% of the calculated E_{O+} values were greater than 50 eV and only 3% of them were grater than 100 eV. The database we used to calculate the average energy does not includes very energetic ion beams and will underestimate energetic conics. We therefore examined the occurrence of energetic ion beams and conics from the non-mass resolving ion instrument, IESA, and found that the sample set we used to calculate the E_{O+} did not significantly affect the statistical result. Specifically, energetic (>100 eV) ion beams were found in the IESA data in ~3% of the intervals for which we have mass analyzed ion data. Thus, energetic ion beams are not common at FAST altitudes and excluding those that occur in low-density regions only slightly reduces the value of the average E_{O+}.

Energetic conics (distributions extending above 100 eV) were found in the IESA data in ~20% of the TEAMS intervals. Very energetic conics (extending above 1 keV) were observed in only 5% of these intervals. Conics are observed in a broader local time region than beams, which are concentrated on the night side. Mirroring energetic plasma sheet O^+ ions are present less frequently than H^+, and are observed primarily near the equatorward side of the oval. Thus, the nighttime maximum near the equatorward boundary of E_{O+} seen in Figure 3c and 3f is real.

The mean E_{O+} increases with altitude (Figure 2a-c and 3a-f) and the highest mean E_{O+} are found in the cusp and at the night sector as shown in Figure 3c. The averaged upward number flux over distributions in which the E_{O+} was determined is larger than that over all distributions since E_{O+} is derived only for distributions with a clear outflow (compare the middle and bottom row in Figure 2).

In the dawn and dusk sectors, both the outflow rates and E_{O+} are lower, but the latitudinal widths of the auroral region are larger when compared to those in the noon and midnight sectors [Andersson *et al.*, 2004]. This means that one needs to also take into account the latitudinal distribution when assessing the relative importance of O^+ mass outflow and associated energy for the different local time sectors when analyzing Figure 3.

The high outflow rates at low altitudes at dusk (~18 MLT) are remarkable (Figure 2d). These high outflow rates are associated with low E_{O+} (Figure 2a), and the high fluxes are also missing at higher altitudes. These facts suggest that this high flux, low energy O^+ population does not acquire escape energy and is therefore gravitationally bound. The investigation of the cause(s) of the dawn/dusk asymmetry in the O^+ energy and outflow profiles suggested in Figure 2 is deferred to a future study.

With the notable exception of the dusk region, Figure 2g-i shows that the observed upward O^+ flux intensity increases with altitude. Peterson *et al.* [2001] and others have suggested that the increase in upward ion flux with altitude arises from the acceleration or energization of thermal ions to energies above an instrumental lower energy threshold. However since the FAST observations above 3000 km have the same total outflowing flux as observations by other satellites, the calculation of E_{O+} for the upper altitude range in Figure 2 and 3 includes the main part of the escaping ion population.

The altitude dependence of O^+ upflowing flux and E_{O+} as a function of relative position in the auroral oval as shown in Figure 3 has been examined through 4 broad MLT regions in Figure 3d-i. With the exception of the low altitude dusk side component discussed above, the highest upflowing fluxes are seen near the poleward auroral oval boundary. In the highest altitude range the difference in flux between the poleward and equatorward edges is about an order of magnitude difference at noon and factor of two at midnight as can be seen in Figure 3i.

The E_{O+} at the lowest altitude range is about ~5 eV everywhere except at midnight, where it is ~30 eV. At higher altitudes E_{O+} is significantly higher, except in the dusk/dawn sectors. The most significant increase in E_{O+} is in the midnight region and between the two highest altitude bins (i.e. above ~3200 km). The altitude dependence of E_{O+} in the noon sector is more complex. Here, at high altitudes, the maximum value of

E_{O+} is not located at the poleward edge of the auroral oval. At the highest altitude range the peak in the E_{O+} and in the outflow flux are not co-located: compare Figure 3f and 3i. The energies of ions in the noon region exhibit a well-known energy dispersion with latitude that arises from large scale convection, and the difference in the relative position in the auroral oval where E_{O+} and outflow fluxes peak is most probably also the net result of convection in the cusp region.

Summary and Discussion

We have presented in Figure 3 estimates of the O^+ characteristic energy (E_{O+}) of the accelerated ion outflow population as a function of altitude (1500-4200 km) and relative location in the auroral oval based on one year of data. Our method is limited by physical and instrumental constraints discussed above. The total outflowing O^+ flux observed above 3000 km by the FAST satellite is equal to reported observations at higher altitudes and therefore the calculated E_{O+} at the high altitudes is representing the main part of the escaping ions.

The method presented here cannot be used to determine the magnitude of the O^+ polar wind energization in the polar cap. Abe *et al*. [2004] presented a comprehensive investigation of the bulk flow as function of longitude and latitude of the O^+ component of the polar wind. We note that at an altitude of 600 (6,000) km O^+ has to have an upward directed energy of greater than 10 (5) eV to reach the plasma sheet. Ions with lower energies fall back into the ionosphere unless energized and are therefore not significantly involved in the formation of the plasma sheet. The lack of significant upflowing O^+ in the TEAMS energy range outside the auroral oval strongly suggests that almost all of the O^+ energized to escape velocity comes from auroral latitudes.

Our principal result is illustrated in Figure 3. We show that the altitude dependence of E_{O+} is distinctly different in the noon, midnight, dusk and dawn. This implies that either different physical processes are dominant, or that the altitude dependences of these processes and the transport of ions are different in these sectors. We noted that Abe *et al.* [2004] reported the highest bulk polar wind velocities are mainly in the dawn and dust sectors. The strongest additional polar wind energization is in this study observed to

occur in the night region, the region which has the least upward bulk polar wind velocity. Other results are noted above.

As noted by Winglee *et al.* [2002] and others, understanding the distribution and energization of heavy ions such as O^+ is required to obtain an accurate picture of global magnetospheric dynamics. The results presented above demonstrate that the process energizing the O^+ component of the polar wind to escape velocity has significant variation in local time, relative position in the auroral zone and altitude that have, so far, not been included in global magnetospheric models.

REF:

Abe T., A. W. Yau, S. Watanabe, M. Yamada and E. Sagawa (2004), Long-term variation of the polar wind velocity and its impact for the ion acceleration process: Akebono/suprathermal ion mass spectrometer observations, J. Geophys. Res., 109, A09305, doi:10,1029/2003JA010223.

Andersson, L., W. K. Peterson, and K. M. McBryde (2004), Dynamic Coordinates for Auroral Ion Outflow, *J. Geophys. Res*., Vol. 109, No. A8, doi:10.1029/2004JA010424.

Carlson, C. W., R. F. Pfaff, and J. G. Watzin, The Fast Auroral SnapshoT (FAST) mission (1998), *Geophys. Res. Lett.,* 25: 2013-2016.

Carlson, C. W., J. P. McFadden, P. Turin, D. W. Curtis and A. Magoncelli (2001), The electron and ion plasma experiment for Fast, *Space Science Reviews.,* 98: 33-66.

Cully, C. M., E. F. Donovan, A. W. Yau, and G.G. Arkos (2003), Akebono/Suprathermal Mass Spectrometer observations of low-energy ion outflow: Dependence on magnetic activity and solar wind conditions, *J. Geophys. Res*., *108*(A2), 1093, doi:10.1029/2001JA009200.

Hultqvist, B. M. Oieroset, G. Paschamann, and R. Treumann (1999), *Magnetospheric Plasma Sources and Losses,* Kluwer, Dordrecht. Chapters in this book also appeared as articles in *Space Science Reviews*, Vol. 88.

Klumpar et al. (2001), The Time-of-Flight Energy, Angle, Mass Spectrograph (Teams) Experiment on Fast, *Space Science Reviews* 98: 197-219.

Lennartsson, O.W., H.L. Collin, and W.K. Peterson (2004), Solar wind control of Earth's H^+ and O^+ outflow rates in the 15-eV to 33-keV energy range, *J. Geophys. Res.*, *109*(A12), 12212, doi:10.1029/2004JA010690.

Miyake, W., T. Mukai and N. Kaya (1993), On the evolution of Ion Conics Along the Field Line From EXOS D, *J. Geophys. Res.*, 98, 11127.

Miyake, W., T. Mukai, and N. Kaya (1996), On the origins of the upward shift of elevated (bimodal) ion conics in velocity space, *J. Geophys. Res., 101*, 26,961.

Peterson, W.K., H.L. Collin, M.F. Doherty, and C.M. Bjorklund (1992), O^+ and He^+ Restricted and Extended (Bi-modal) Ion Conic Distributions, *Geophys. Res. Lett.,* 19, 1439.

Peterson, W.K., H.L. Collin, M.F. Doherty, and C.M. Bjorklund (1995), Extended (Bi-Modal) Ion Conics at High Altitudes, , in Space Plasmas: Coupling Between Small and Medium Scale Processes, Geophysical Monograph #86, M. Ashour-Abdalla, T. Chang, and P. Duesenbery (Eds.), American Geophysical Union, pg. 105.

Peterson, W. K., H. L. Collin, A. W. Yau and O. W. Lennartsson (2001), Polar/Toroidal Imaging Mass-Angle Spectrograph observations of suprathermal ion outflow during solar minimum conditions, *J. Geophys. Res.*, 106, 6059.

Winglee, R. M., D. Chua, M. Bittnacher, G. K. Parks, and G. Lu (2002), Global impact of ionospheric outflows on the dynamics of the magnetosphere and cross-polar cap potential, *J. Geophys. Res.*, 107(A9), 1237, doi:10,1029/2001JA000214.

Yau, A.W., and M. André (1997), Sources of ion outflow in the high latitude ionosphere, *Space Sci. Rev., 80*, 1.

Figure 1: Example of energetic ion outflow. Panel (a) and (b) represents the earthward and anti-earthward oxygen energy spectrograms. Panel (c) the number flux of outflowing

oxygen ions. Panel (d) the calculated O^+ density. See text for details about the various lines in the panels.

Figure 2: The ion outflow and E_{O+} as function of ILAT and MLT. Invariant latitude of 60, 70 and 80 degrees are marked in the figures by the circles. Noon is at the top of the page and dusk is to the left. Small dials represents the number of measurements in each pixel and the large dials the respective quantity. The columns represents three different altitude ranges and rows represents E_{O+}, the ion outflow for the calculated E_{O+} and the ion outflow from all measurements.

Figure 3: The ion outflow and E_{O+} as function of location in auroral oval and MLT. The data is presented for three different altitude ranges (columns) and with the information about the E_{O+} (row 1 and 2) and the flux for the events where E_{O+} could be determined. The top row presents the E_{O+} as function of ILAT and location in aurora oval. The second row is the same data but presented as line plots for four different MLT bins as indicated in figure. The third row is the ion flux.
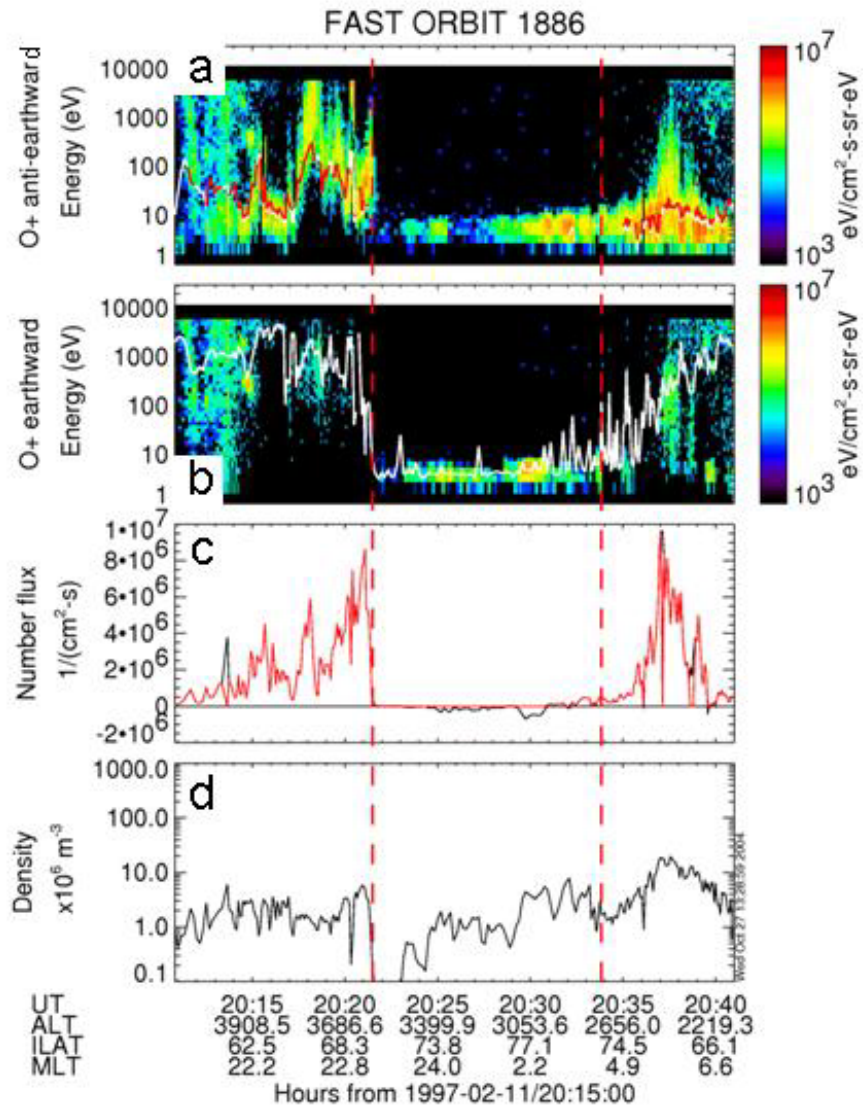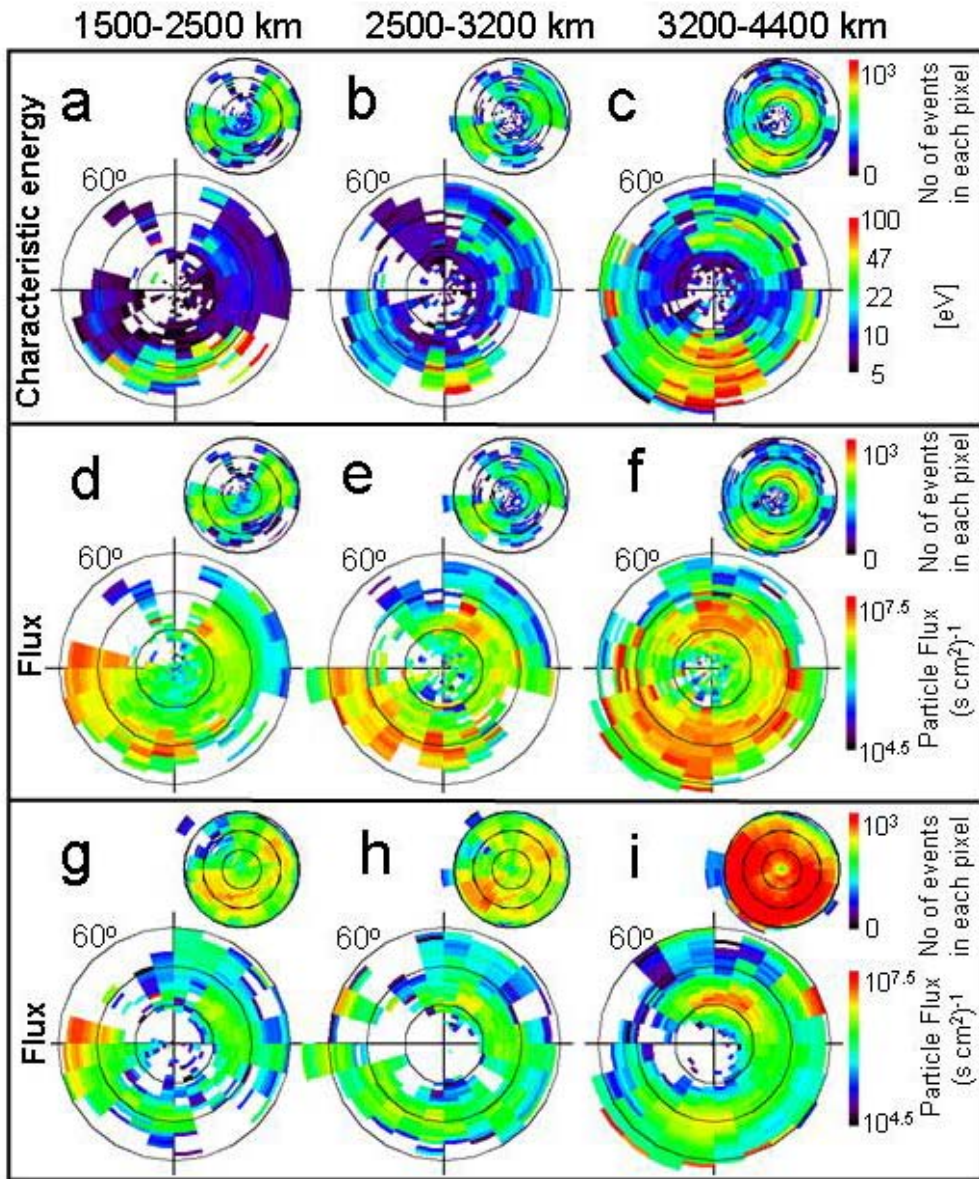
Figure 1:

Figure 2:

Figure 3: